Applied Surface Science 257 (2011) 7732–7738

Contents lists available at ScienceDirect

Applied Surface Science

journal homepage: www.elsevier.com/locate/apsusc

Study of the corrosion products formed on a multiphase CuAlBe alloy in a sodium chloride solution by micro-Raman and in situ AFM measurements

S. Montecinos[a,b,*], S.N. Simison[a,b]

[a] INTEMA, Facultad de Ingeniería, Universidad Nacional de Mar del Plata, Juan B. Justo 4302, 7600 Mar del Plata, Argentina
[b] CONICET, Argentina

ARTICLE INFO

Article history:
Received 9 February 2011
Received in revised form 31 March 2011
Accepted 3 April 2011
Available online 12 April 2011

Keywords:
In situ AFM
Micro-Raman spectroscopy
Copper-based alloys
Corrosion
Microstructure

ABSTRACT

The corrosion products formed on a multiphase Cu–11.40Al–0.55Be (wt.%) alloy in 3.5% NaCl at open circuit potential, and their evolution with immersion time were studied mainly by micro-Raman and in situ AFM measurements. The aluminium content of each phase affects the formation of the corrosion products on them. After 1 day of immersion, γ_2 precipitates were more susceptible to dealuminization, while α' phase exhibited a high corrosion stability. The corrosion products evolved with immersion time, and $CuCl_2$ and a Cu_2O/CuO double layer film were the stable products formed on all the phases after long times.

1. Introduction

Cu–Al–Be system has been developed as a shape memory alloy (SMA) by adding small quantities of beryllium into eutectoid Cu–(11.4–11.8 wt.%)Al system, in order to decrease the martensitic transformation temperature and thereby obtain the pseudoelastic behaviour at room temperature [1–4]. These alloys are highly promising for applications as passive dampers of seismic energy in structural frames of buildings or in bridges [2,5].

The pseudoelastic behaviour can be modified, among other several factors, by the formation of precipitates [6]. Two types of precipitates can be observed in copper-based SMAs after aging treatments: α' phase in hypoeutectoid system and γ_2 phase in hypereutectoid system. For Cu–Al–Be alloys with an isothermal treatment between 400 and 490 °C, the formation of α' phase followed by the eutectoid decomposition ($\beta \rightarrow \alpha' + \gamma_2$) has been obtained [7].

Montecinos and Simison [8] studied the corrosion behaviour of β and ($\beta + \gamma_2$) microstructures of a shape memory Cu–Al–Be alloy. Chloride-rich environments can produce dealuminization attack and the corrosion behaviour is affected by the alloy microstructural conditions. After long times of immersion, the single β phase microstructure suffers localized corrosion in some regions but dealuminization is generalized on the whole surface. However, in the ($\beta + \gamma_2$) microstructure preferential dissolution of γ_2 dendritic precipitates occurs, which seems to protect β matrix from de-alloying [8]. Han et al. [9] investigated the corrosion mechanism of a Cu–9Al–2Mn (wt.%) alloy, which exhibit a structure consisting of α and the eutectoid phase. They demonstrated that α phase did not show any change after 3 years of immersion in a marine environment, while the eutectoid structure suffered a preferential corrosion attack. Rosatto et al. [10] studied the electrochemical behaviour of Cu–Al–Ag alloys, and they found that γ_1 phase and the ($\gamma_1 + \alpha_1$) structure are the preferred attacked phases, while α_1 phase would be the area where the cathodic reaction occurs.

The in situ tapping mode atomic force microscopy (AFM) has proven to be a very valuable tool for the analysis of thin films of oxides formed on metal surfaces and it provides quantitative measurements of the surface topography. In addition, this technique allows direct in situ measurements during the corrosion process taking place under controlled conditions [9,11]. Using this technique together with other ex situ measurements, which allows the identification of the corrosion products formed on the surface samples, it is possible to obtain a more accurate view of the evolution of the surface over time.

In situ AFM results of the first stages of corrosion of a multiphase shape memory Cu–Al–Be alloy in 3.5% NaCl are presented. The identification of the reaction products formed on each phase

* Corresponding author at: INTEMA, Facultad de Ingeniería, Universidad Nacional de Mar del Plata, Corrosion Division, Juan B. Justo 4302, 7600 Mar del Plata, Argentina.
E-mail addresses: dmonteci@exa.unicen.edu.ar, dmonteci@fi.mdp.edu.ar (S. Montecinos).

0169-4332/$ – see front matter © 2011 Elsevier B.V. All rights reserved.
doi:10.1016/j.apsusc.2011.04.018

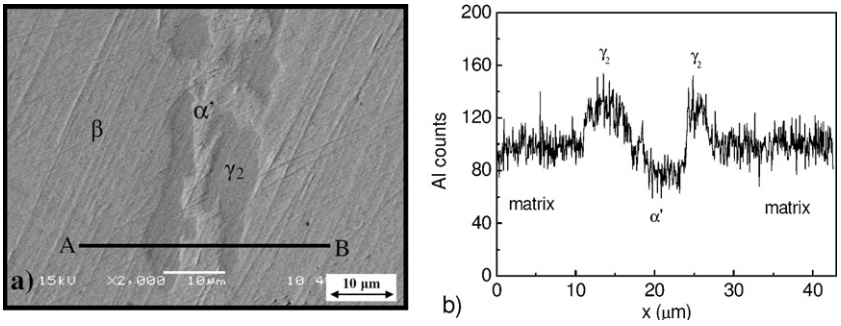

Fig. 1. (a) Micrograph of a sample before the immersion (backscattered electrons-SEM); (b) aluminium compositional profile along the line A–B in Fig. 1a.

was done by ex situ micro-Raman measurements, jointly with other techniques, for immersion times in the range of 1–65 days.

2. Experimental procedure

The Cu–11.40Al–0.55Be (wt.%) polycrystalline alloy under study was obtained from Trefimetaux (France) as 15 mm diameter extruded bars. The chemical composition was determined by atomic absorption spectrophotometry. Prior to performing the heat treatment, the samples were previously heated during 5 min at 800 °C in the β field and water quenched at room temperature (single β phase microstructure). Precipitation of α′ phase was generated by an isothermal aging treatment at 505 °C, followed by water quenching at room temperature. A detailed description is given in [7]. The temperature was monitored using a chromel–alumel thermocouple. The software Image Tool 3.0 was used to estimate the volume fraction of precipitates in the specimens as the relative area occupied by them with respect to the total area. The samples were smoothed with 240, 600 and 1000 grit emery paper and then polished with alumina powder (0.3 μm size).

For corrosion tests specimens were immersed in a 3.5% NaCl solution adjusted to pH 8 with borate–boric acid buffer for different exposure times in the range of 1–65 days. The solution was maintained at room temperature (20 ± 2 °C) and air was bubbled through it. After the immersion, the samples surfaces were rinsed gently with distilled water, sprayed with ethanol and dried with hot air.

The surface morphology of the samples before and after immersion in the chloride solution was examined using an Olympus PMG3 optical microscope (OM) and a JEOL JSM-6460LV scanning electron microscopy (SEM). Energy dispersive X-ray spectroscopy (EDX) analysis under SEM was employed to obtain an estimation of the surface composition of different regions of the samples and their variability was obtained as the standard deviation of at least three experimental measurements. The beryllium content could not be detected by this technique. X-ray diffraction (XRD) using a PANanalytical X'Pert Pro PW3373 equipment with low incidence angle (3°) was used to identify the phase structure of specimens before the immersion and of the corrosion product films formed after that. It was operated at 40 kV and 40 mA with the excitation of CuK_α ($\lambda = 1.54056$ Å).

Tapping mode atomic force microscopy (AFM) using an Agilent 5500 microscope was employed to study in situ the changes of the sample surfaces immersed in 3.5% NaCl adjusted to pH 8 during 21.5 h at open circuit potential.

Corrosion products after 1, 21 and 65 days of immersion at open circuit potential were locally characterized by micro-Raman spectroscopy (Invia Reflex confocal Raman Microprobe). The incident beam was focused on the specimens as a spot size diameter of 1 μm (high confocality mode). Excitation was provided with the 514 nm emission line of an Ar^+ laser and measurements were performed in backscattering configuration using a 50× objective.

3. Results and discussion

3.1. Microstructural characterization

α′ phase was formed in the samples by the isothermal aging treatment. Small quantities of γ_2 phase in some zones surrounding α′ were also obtained. A volume fraction of 1.2 ± 0.5% of α′ phase and 0.8 ± 0.6% of γ_2 phase was estimated from optical micrographs. The precipitates were difficult to distinguish on polished samples using the detector of secondary electrons in SEM. However, they could be observed by backscattered electrons, which provided information about the distribution of the alloying elements in the sample (Fig. 1a). The darker areas could be associated with a composition with lower atomic mass, which agree with EDX results (Table 1). Copper rich α′ phase (Table 1) was located mainly in the grain boundary zones. In some regions surrounding the α′ phase, dark precipitates, which correspond to γ_2 phase were distinguished (Fig. 1a and Table 1). Fig. 1b shows a compositional profile of aluminium along the line A–B in Fig. 1a. It can be clearly seen that α′ phase is poorer, while γ_2 phase is richer in aluminium than the matrix.

The XRD patterns of the samples before the immersion (Fig. 2b) confirmed the presence of γ_2 precipitates with a Cu_9Al_4 structure in a β DO_3 matrix and some β′ martensite phase. The presence

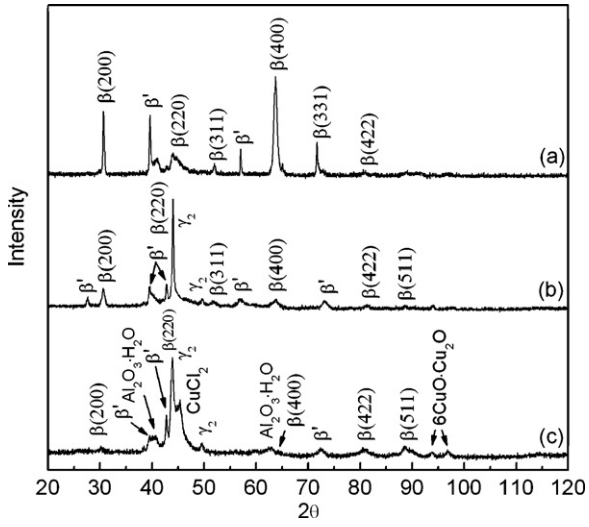

Fig. 2. XRD patterns of: (a) blank β sample; (b) (β + α′ + γ_2) sample before immersion; and (c) (β + α′ + γ_2) sample after 24 h of immersion in 3.5% NaCl. All the measurements were obtained at low incidence angle (3°).

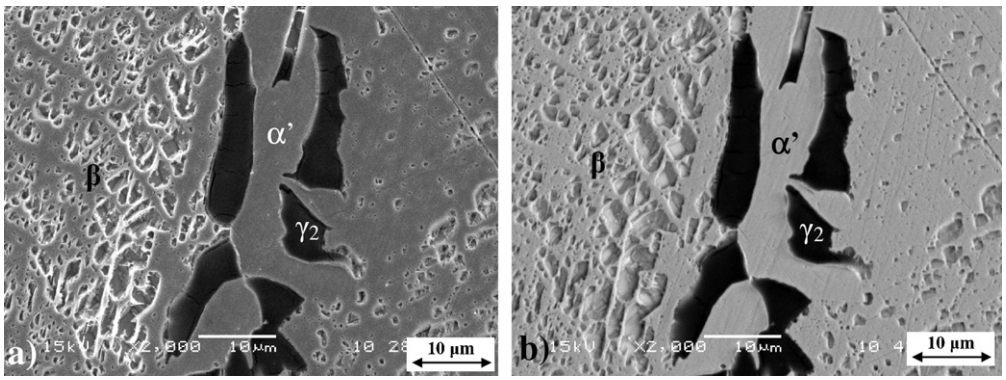

Fig. 3. Micrographs of the samples after 24 h of immersion in 3.5% NaCl by SEM: (a) secondary electrons and (b) backscattered electrons.

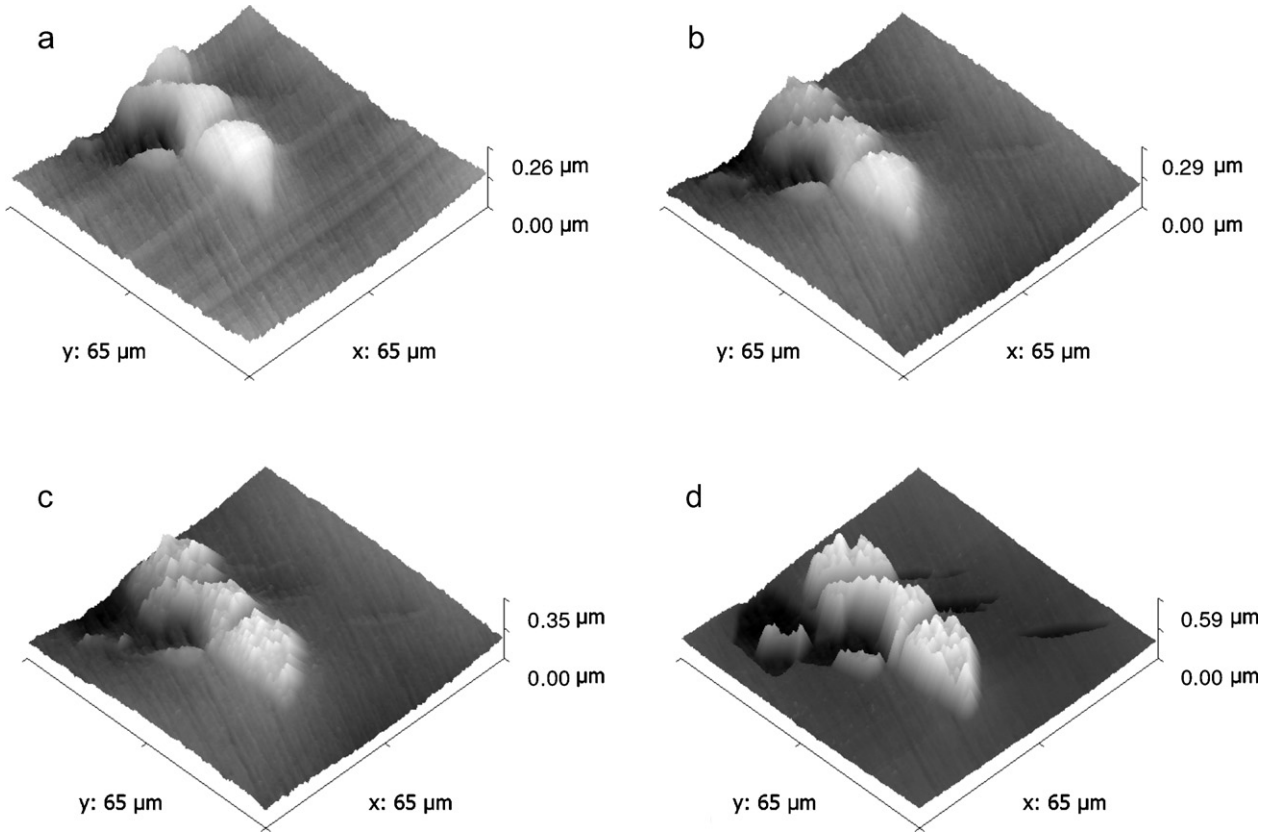

Fig. 4. Three-dimensional AFM topographic images of the Cu–Al–Be sample surface after (a) 0.5 h, (b) 11 h, (c) 16 h and (d) 21.5 h of exposure to a 3.5% NaCl solution.

of some retained martensite phase in the surface of the samples could be due to the deformation produced during polishing. The crystal structure of α′ precipitates in a hypoeutectoid Cu–Al–Be alloy has been identified to be 18R long period stacking order structure, similar to that of the β′ martensite phase [12]. For that reason, both phases are difficult to differentiate from diffraction patterns [12,13]. The XRD patterns of a blank β sample (Fig. 2a) showed the presence of some martensite phase, however, more peaks attributed to β′ were found for the (β + α′ + γ2) sample (Fig. 2b), which could be ascribed to the presence of α′ phase.

Table 1
EDX measurements before and after 24 h of immersion in 3.5% NaCl.

Element	Mass concentration (wt.%)					
	Before immersion			After 24 h immersion		
	Matrix	α′	γ2	Matrix	α′	γ2
Cu	85.2 ± 0.3	88.4 ± 0.7	81.7 ± 0.3	86.2 ± 0.3	88.7 ± 0.1	27.1 ± 6.4
Al	14.8 ± 0.3	11.6 ± 0.7	18.3 ± 0.3	13.8 ± 0.3	11.1 ± 0.1	35.2 ± 2.8
O						36.8 ± 3.8
Cl						0.9 ± 0.1

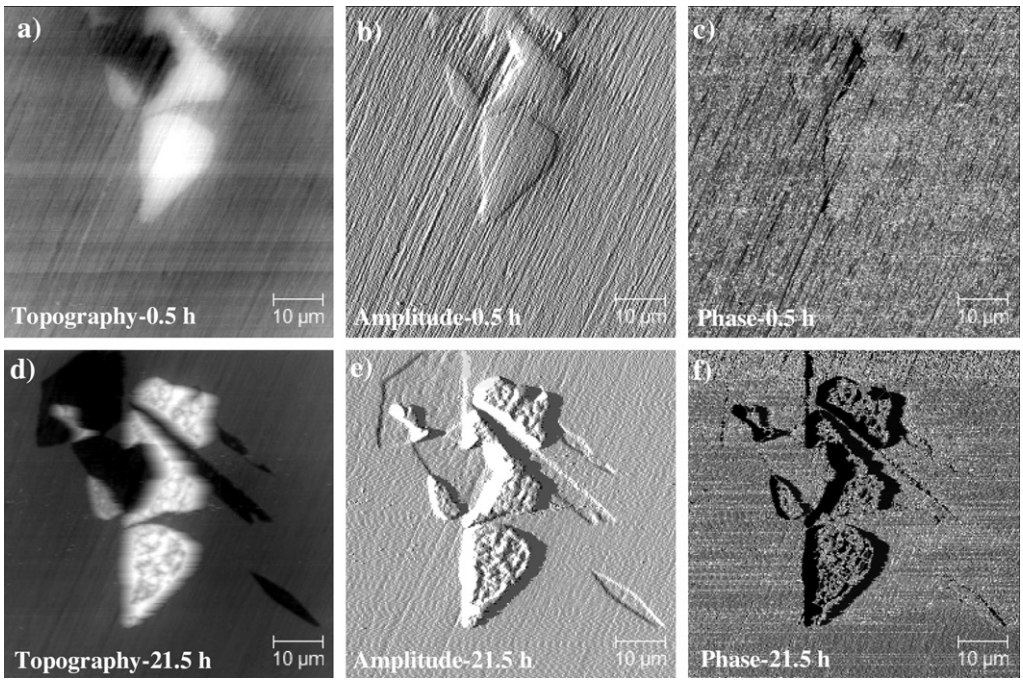

Fig. 5. AFM images of topography (a and d), amplitude (b and e) and phase (c and f) of the Cu–Al–Be sample surface after 0.5 h and 21.5 h of exposure to a 3.5% NaCl solution.

3.2. Short duration immersion tests

After 24 h of immersion in 3.5% NaCl, γ_2 precipitates were clearly visible and presented as dark zones (Fig. 3). A surface film rich in O and Al formed on γ_2 precipitates (Table 1), which would correspond to $Al_2O_3{\cdot}H_2O$, as was identified by XRD measurements (Fig. 2c). Small quantities of Cl were also detected by EDX (Table 1), which could be associated to the presence of $CuCl_2$ (Fig. 2c). The high values of the EDX measurements dispersion for γ_2 phase could be associated to differences in the thick and rates of formation of the corrosion products produced on different precipitates.

The matrix was slightly impoverished in Al (Table 1), and some surface changes produced by the corrosion process, were observed in the SEM micrographs (Fig. 3). The formation of corrosion products on α' phase after the immersion was not detected by EDX measurements (Table 1) or in the SEM micrographs (Fig. 3), which would indicate that this phase has a higher corrosion stability. Also, the presence of $6CuO{\cdot}Cu_2O$ was found on the sample surfaces (Fig. 2c).

In situ AFM studies were used to study in detail the progress of dissolution and formation of the corrosion products on the surface of each phase in the ($\beta + \alpha' + \gamma_2$) microstructure. During the time of immersion, AFM images were registered on line. A representative selection of them is presented in Fig. 4. The first one at $t = 30$ min (Fig. 4a) corresponds to the first scan obtained after the adjustments for the correct acquisition of the images. Note that polishing scratches are clearly visible and therefore it can be assumed that the sample surface had not yet been altered by the solution and then, it was considered as the blank. The phases could be distinguished from the topography: γ_2 precipitates are higher than the β matrix (light zones), while α' phase is lower than the matrix (dark zones). The dissimilarities in height of the phases respect to the matrix in the first image would be produced during the polishing process, due to the differences in their respective hardness. γ_2 precipitates are the hardest phase, while the α' phase is the softest one [14].

A qualitative analysis of the evolution of topographic images in Fig. 4 gave some information about the changes undergone by the surface with immersion time:

(a) The formation of corrosion products on the matrix would give place to a smoother surface (the polishing scratches were difficult to find after 21.5 h of exposure).
(b) A surface film of corrosion products grew on γ_2 precipitates.
(c) A seeming decrease of the α' phase height.

Fig. 5 shows the AFM images of topography, amplitude and phase of the sample surface that has been exposed to a 3.5% NaCl solution for 0.5 h (Fig. 5a–c) and 21.5 h (Fig. 5d–f). The topography and amplitude images are associated to the morphology of the sample surface, while the phase image is the mapping of the changes in the phase angle of the cantilever oscillation during the tapping mode scan, and contrast variations in this image can be associated to changes in the properties of the sample surface [15]. Consequently, it could be deduced that a new compound with a different composition grew on γ_2 precipitates (Fig. 5a and d). On the other hand, the decrease in height of α' phase (Fig. 5a and d) could not be related to any significant change in the composition of this zone (Fig. 5c and f).

Fig. 6 shows some representative surface depth profiles obtained from the topographic AFM images at different immersion times along selected lines. Those lines were indicated in each case in the topographic image obtained after 21.5 h of immersion. It is important to note that the profiles could present a slight drift in z. After 21.5 h, a surface film of corrosion products with a thickness of around 0.3 μm grew on γ_2 precipitates (Fig. 6a). α' phase remained almost unchanged (Fig. 6a), which is in agreement with EDX measurements in Table 1. Then, the height difference between α' and the matrix can be attributed to the formation of corrosion products with a thickness of 0.1 μm on the last one (Fig. 6a and b).

For a better identification of the corrosion products formed on each phase at each immersion time, micro-Raman spectra were measured after 24 h of immersion at open circuit potential. At least three spectra of each phase were measured with very good reproducibility. Fig. 7 shows representative spectra corresponding to the β matrix, γ_2 precipitates and α' phase. The frequency shift of the main peaks is indicated in the curves. The presence of the peaks at 337 and 620 cm^{-1} and the absence of the peaks at around 150 and

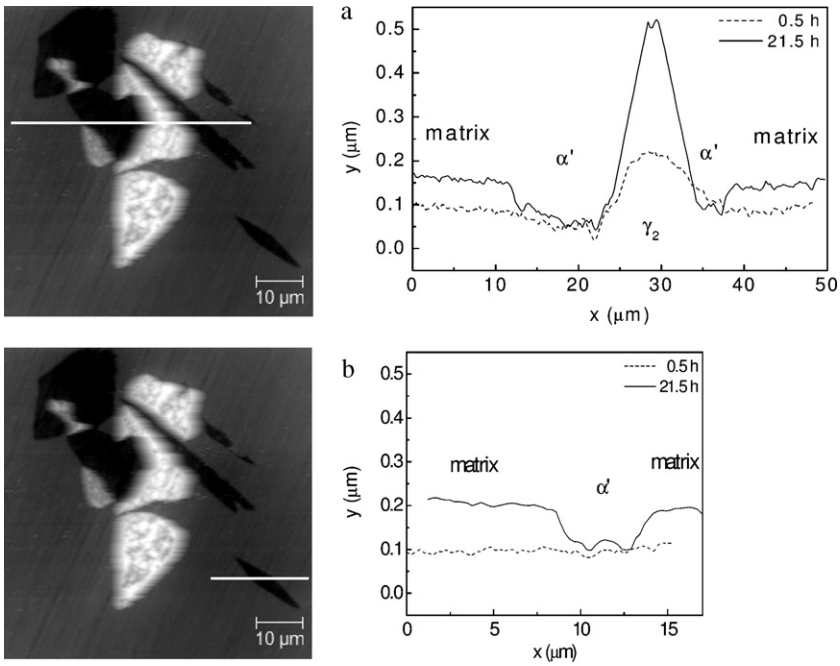

Fig. 6. Surface depth profiles of the topographic images at different immersion times along selected lines.

220 cm^{-1} on the matrix surface indicated the formation of CuO [16]. However, Cu_2O could be also identified in spectra corresponding to other zones of the matrix (peaks at 147, 217 and 630 cm^{-1} [16]), which is consistent with the XRD patterns indicated the formation of $6CuO{\cdot}Cu_2O$ (Fig. 2c). Then, the results suggest the existence of a duplex film. The formation of this Cu_2O/CuO double layer has been reported previously in copper samples immersed in chloride containing solutions [17,18]. The presence of $CuCl_2$ was also identified on some zones of the matrix (peak at 287 cm^{-1} [19]), in agreement with XRD measurements (Fig. 2c). No chlorine compounds could be detected by EDX (Table 1), which would indicate that $CuCl_2$ is present in small quantities in some zones or forming a very thin film. From the results, the decrease in surface roughness on the matrix measured by AFM would be attributed to the formation of a surface film composed of CuO, Cu_2O and $CuCl_2$.

The existence of Al_2O_3 (peak at 419 cm^{-1} [19,20]) and Cu_2O (peaks at 147, 217, 531 and 635 cm^{-1} [16]) on γ_2 precipitates was confirmed by micro-Raman measurements (Fig. 7). Corrosion products containing Cl were measured by EDX (Table 1), while they were not detected by micro-Raman measurements. Based on the fact that the measurements obtained by micro-Raman are more superficial than those obtained by XRD [21,22], the results suggest that the film formed on γ_2 precipitates would be composed superficially of Al_2O_3 and Cu_2O, with $CuCl_2$ underneath it.

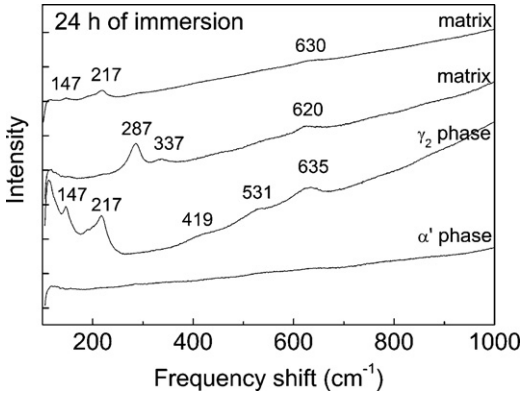

Fig. 7. Micro-Raman spectra collected from sample after 24 h of exposure to a 3.5% NaCl solution.

It was not possible to identify corrosion products on α′ phase (Fig. 7), which is in agreement with the high stability found by SEM, EDX and AFM measurements (Table 1 and Figs. 3–6). If there was a film of corrosion products on α′ phase, it would be very thin.

It could be observed that during the early stages of immersion, γ_2 precipitates were more susceptible to dealuminization and to the formation of Al_2O_3 on them (Cu_2O and $CuCl_2$ were also identified). This could be explained considering that γ_2 precipitates are the aluminium rich phase, and so they would be the most anodic [8,10]. It has been previously reported that the de-alloying rate of aluminium from the Cu–Al alloys surface increases in proportion to the aluminium content in the alloys [23]. On the β matrix, a Cu_2O/CuO surface film and $CuCl_2$ were formed. It was found that α′ phase has a high corrosion stability, which can be due to the fact that α′ was the aluminium poorest phase.

3.3. Long duration immersion tests

To study the evolution of the corrosion products formed on the surface samples after long immersion times, microscopical and micro-Raman measurements were done after 21 and 65 days of immersion. It could be observed that the β matrix suffered a visible corrosion process (Fig. 8), but it seems not to be so severe as the single β phase samples submitted to a similar solution and conditions after 40 days [8]. A surface film composed of CuO (peaks at 333 and 618 cm^{-1} [16]) and $CuCl_2$ (peak at 281 cm^{-1} [19]) was identified on it (Fig. 9b).

α′ phase still seemed to remain almost unchanged (Fig. 8), but the formation of some corrosion products could be detected after 21 days: Cu_2O (peaks at 151, 216, 537 and 639 cm^{-1} [16]), and $CuCl_2$ (a slight peak at 288 cm^{-1} [19]) (Fig. 9a). They evolved with the immersion time, and the presence of CuO (peaks at 333 and 618 cm^{-1} [16]) and $CuCl_2$ (peak at 288 cm^{-1} [19]) was identified after 65 days (Fig. 9b).

After 21 days, Cu_2O (peaks at 149, 219, 537 and 634 cm^{-1} [16]) and $CuCl_2$ (a slight peak at 291 cm^{-1} [19]) could be identified on

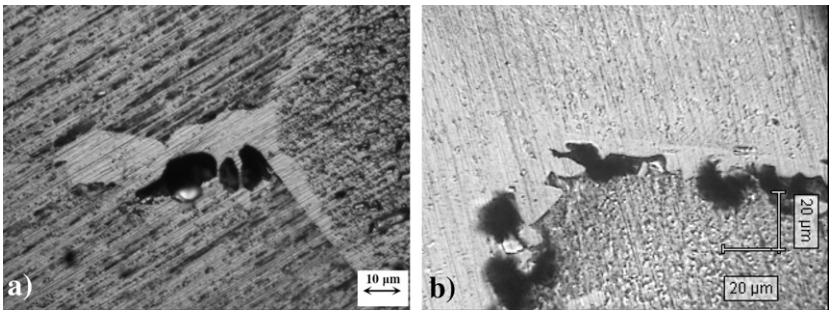

Fig. 8. Optical micrographs of the samples after (a) 21 days and (b) 65 days of exposure to a 3.5% NaCl solution.

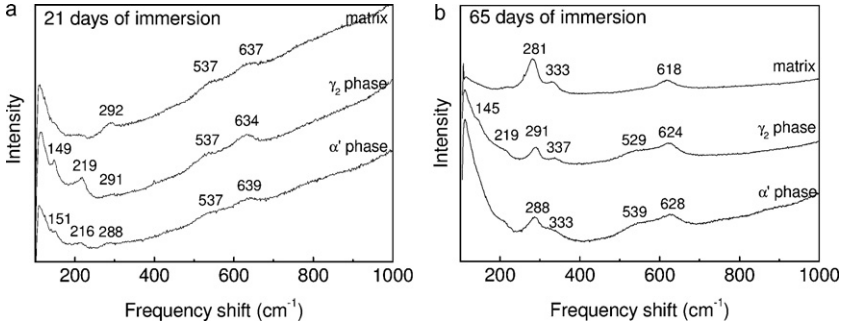

Fig. 9. Micro-Raman spectra collected from samples after (a) 21 days and (b) 65 days of exposure to a 3.5% NaCl solution.

γ_2 phase (Fig. 9a), and the presence of Al_2O_3 could not be detected (Fig. 9a). This compound seemed to have been detached from those precipitates. A similar behaviour has been reported previously in a ($\beta + \gamma_2$) sample [8]. After 65 days, $CuCl_2$ (peak at 291 cm^{-1} [19]) was detected, peaks associated to Cu_2O (at 145 and 219 cm^{-1} [16]) became weaker and the presence of a peak at 333 cm^{-1} suggested the existence of CuO [16] (Fig. 9b).

The obtained results point that the aluminium content of each phase affects the corrosion products formed on them, as well as their formation rate, however, they evolve to the same compounds after long immersion times. $CuCl_2$ and a Cu_2O/CuO double layer surface film were formed on the β matrix. Kear et al. [17] has reported a Pourbaix diagram for copper in seawater of salinity 3.5% at 25 °C considering that the solid phases are Cu, Cu_2O, CuO, CuCl and $Cu_2(OH)_3Cl$. In solutions with pH 8, the equilibrium corrosion product is Cu_2O.

For copper, it has been established [17] that in aerated chloride media the main corrosion process is its dissolution to form a dichlorocuprous anion complex, which is generally simplified to:

$$Cu + 2Cl^- \rightarrow CuCl_2^- + e^- \quad (1)$$

As the local concentration of $CuCl_2^-$ increases, it can be expected that cuprous oxide is deposited in the surface by a dissolution/precipitation process [17]:

$$2CuCl_2^- + 2OH^- \rightarrow Cu_2O + H_2O + 4Cl^- \quad (2)$$

It is also proposed that in seawater Cu_2O generally oxidizes over time to CuO, mainly due to the oxygen present in the water [17,23]. These results are in agreement with the presence of the duplex layer found in the surface of the samples under study, with CuO in the outside part due to the oxidation of Cu_2O. After long immersion times, only CuO was clearly detected on the matrix surface by micro-Raman, but some quantities of Cu_2O could be in the inner part of the corrosion product layer, which can not be detected by this technique. The presence of $CuCl_2$ in the corrosion products has been also reported by other authors. Peng et al. [24] found that the corrosion products of copper in sea water are mainly CuCl and $CuCl_2$, and Chmielová et al. [25] identified $Cu_2(OH)_3Cl$ and $CuCl_2$ on a copper surface after a four days treatment in sodium/magnesium chloride solution. No $Cu_2(OH)_3Cl$ and CuCl were detected in the samples studied in this work. $CuCl_2$ could be formed on the samples surfaces by the following reaction [26]:

$$Cu^{2+} + 2Cl^- \rightarrow CuCl_2 \quad (3)$$

Al_2O_3 was formed on the richest aluminium phase, γ_2, probably due to the complexation of aluminium by chloride, followed by hydrolysis [27]. However, this compound seems not to be stable after long immersion times and to have been detached from the precipitates. Cu_2O and $CuCl_2$ were also identified, and the last one would be in the inside part of the corrosion product layer. It agrees with measurements after longer immersion times, where $CuCl_2$ was detected by micro-Raman after the Al_2O_3 film was detached from the surface. The Cu_2O/CuO double layer surface film was also identified after long immersion times.

On the other hand, the poorest aluminium phase, α′, seems to have a greater stability and corrosion products were not detected on it during the early stages of immersion. But, Cu_2O and CuO were identified by micro-Raman after 21 and 65 days immersion, respectively. Then, it can be inferred that a Cu_2O/CuO duplex layer surface film was also formed on α′ phase after longer immersion times. $CuCl_2$ was also detected.

The above results indicate that the stable corrosion products formed on all the phases after long times of immersion are $CuCl_2$ and a Cu_2O/CuO double layer surface film.

4. Conclusions

The corrosion products formed on a multiphase shape memory Cu–11.40Al–0.55Be (wt.%) polycrystalline alloy in 3.5% NaCl adjusted to pH 8 at open circuit potential, and their evolution with immersion time were studied mainly by micro-Raman and in situ AFM measurements. Samples with a structure consisting of a β matrix, α′ phase located mostly in the grain boundary zones, and

small quantities of γ_2 precipitates in some zones surrounding α' were employed.

The use of in situ AFM jointly with ex situ micro-Raman measurements, which permit the identification of the reaction products formed on each phase, was found to be a great complement for the corrosion studies.

The obtained results point that the aluminium content of each phase affects the development of the corrosion products on them, as well as their formation rate. After 1 day of immersion, $CuCl_2$ and a Cu_2O/CuO double layer surface film were formed on the β matrix. However, γ_2 precipitates (the aluminium rich phase) were more susceptible to dealuminization and to the formation of Al_2O_3 on them, and α' phase exhibited a high corrosion stability and remained almost unchanged. The corrosion products evolved with immersion time, the Al_2O_3 film seemed to have been detached from γ_2 precipitates, and some products were formed on α' phase.

The stable corrosion products formed on all the phases after long times of immersion were $CuCl_2$ and a Cu_2O/CuO double layer surface film.

Acknowledgements

The authors acknowledge the financial support of the CONICET and the University of Mar del Plata, Argentina. They would also like to thank Dr. Beatriz Valcarce for her collaboration with the micro-Raman measurements.

References

[1] S. Montecinos, A. Cuniberti, Thermomechanical behavior of a CuAlBe shape memory alloy, J. Alloys Compd. 457 (2008) 332–336.
[2] S. Montecinos, A. Cuniberti, Aplicación de aleaciones con memoria de forma CuAlBe en amortiguamiento pasivo de estructuras civiles, Rev. SAM 6 (3) (2009) 20–29.
[3] S. Montecinos, A. Cuniberti, A. Sepúlveda, Grain size and pseudoelastic behaviour of a Cu–Al–Be alloy, Mater. Charact. 59 (2) (2008) 117–123.
[4] S. Belkahla, H. Flores Zuñiga, G. Guenin, Elaboration and characterization of new low temperature shape memory Cu–Al–Be alloys, Mater. Sci. Eng. A 169 (1993) 119–124.
[5] R. Desroches, B. Smith, Shape memory alloys in seismic resistant design and retrofit: a critical review of their potential and limitations, J. Earthquake Eng. 7 (3) (2003) 1–15.
[6] A. Cuniberti, S. Montecinos, F.C. Lovey, Effect of γ_2-phase precipitates on the martensitic transformation of a β-CuAlBe shape memory alloy, Intermetallics 17 (2009) 435–440.
[7] S. Montecinos, A. Cuniberti, M.L. Castro, Kinetics of isothermal decomposition in polycrystalline β CuAlBe alloys, Intermetallics 18 (2010) 36–41.
[8] S. Montecinos, S.N. Simison, Influence of the microstructure on the corrosion behaviour of a shape memory Cu–Al–Be alloy in a marine environment, Appl. Surf. Sci. 257 (7) (2011) 2737–2744.
[9] Z. Han, Y.F. He, H.C. Lin, H. Zhao, Dealloying characterizations of Cu–Al alloy in marine environment, J. Mater. Sci. Lett. 19 (2000) 393–395.
[10] S.S. Rosatto, P.L. Cabot, P.T.A. Sumodjo, A.V. Benedetti, Electrochemical studies of copper–aluminum–silver alloys in 0.5 M H_2SO_4, Electrochim. Acta 46 (2001) 1043–1051.
[11] C. Kleber, M. Rosner, H. Hutter, M. Schreiner, Influence of increasing zinc contents in brass in the early stages of corrosion investigated by in-situ TM-AFM and SIMS, Anal. Bioanal. Chem. 374 (2002) 338–343.
[12] H.H. Kuo, W.H. Wang, Y.F. Hsu, Microstructural characterization of precipitates in Cu–10 wt.%Al–0.8 wt.%Be shape-memory alloy, Mater. Sci. Eng. A 430 (2006) 292–300.
[13] P.R. Swann, H. Warlimont, The electron-metallography and crystallography of copper–aluminum martensites, Acta Metall. 11 (1963) 511–527.
[14] L. Wen-sheng, W. Zhi-ping, L. Yang, G. Yong, X. Jian-lin, Preparation, mechanical properties and wear behaviours of novel aluminium bronze for dies, Trans. Nonferrous Met. Soc. China 16 (2006) 607–612.
[15] Agilent Technologies. <www.afmuniversity.org> (last accessed 12.01.11).
[16] G. Niaura, Surface-enhanced Raman spectroscopic observation of two kinds of adsorbed OH^- ions at copper electrode, Electrochim. Acta 45 (2000) 3507–3519.
[17] G. Kear, B.D. Barker, F.C. Walsh, Electrochemical corrosion of unalloyed copper in chloride media—a critical review, Corros. Sci. 46 (2004) 109–135.
[18] Y. van Ingelgen, A. Hubin, J. Vereecken, Investigation of the first stages of the localized corrosion of pure copper combining EIS, FE-SEM and FE-AES, Electrochim. Acta 52 (27) (2007) 7642–7650.
[19] Raman Spectroscopic Library of the National Institute of Advances Industrial Science and Technology (AIST). <http://riodb.ibase.aist.go.jp/riohomee.html> (last accessed 12.01.11).
[20] J.E. Villareal-Barajas, L. Escobar-Alarcón, E. Camps, P.R. González, E. Villagrán, Thermoluminiscence response of aluminium oxide thin films to beta-particle and UV radiation, Superficies Vacío 13 (2001) 126–129.
[21] A.J. Vázquez, J.J. de Damborenea, Ciencia e Ingeniería de la superficie de los materiales metálicos, Ediciones CSIC, Colección Textos Universitarios N° 31, Madrid, 2000.
[22] V.S. Sastri, Corrosion Inhibitors: Principles and Applications, John Wiley and Sons Ltd., Chichester, England, 1998.
[23] A.M. Alfantazi, T.M. Ahmed, D. Tromans, Corrosion behaviour of copper alloys in chloride media, Mater. Des. 30 (2009) 2425–2430.
[24] Z. Peng, G. Bin, J. Yong-ping, Ch. Shu-kang, Corrosion characteristics of copper in magnetized sea water, Trans. Nonferrous Met. Soc. China 17 (2007) s189–s193.
[25] M. Chmielová, J. Seidlerová, Z. Weiss, X-ray diffraction phase analysis of crystalline copper corrosion products after treatment in different chloride solutions, Corros. Sci. 45 (2003) 883–889.
[26] M. Wang, Y. Zhang, M. Muhammed, Critical evaluation of thermodynamics of complex formation of metal ions in aqueous solutions. III. The system Cu(I.II)–Cl^-e at 298.15 K, Hydrometallurgy 45 (1997) 53–72.
[27] A.V. Benedetti, P.T.A. Sumodjo, K. Nobe, P.L. Cabot, W.G. Proud, Electrochemical studies of copper, copper–aluminium and copper–aluminium–silver alloys: impedance results in 0.5 M NaCl, Electrochim. Acta 40 (16) (1995) 2657–2668.